Density-functional study of the cubic-to-rhombohedral transition in α-AlF_3

Yiing-Rei Chen,[1] Vasili Perebeinos,[2,*] and Philip B. Allen[1,3]
[1]*Department of Physics and Astronomy, State University of New York, Stony Brook, New York 11794-3800, USA*
[2]*Department of Physics, Brookhaven National Laboratory, Upton, New York 11973-5000, USA*
[3]*Department of Applied Physics and Applied Mathematics, and the Materials Research Science and Engineering Center, Columbia University, New York, New York 10027, USA*

(Received 14 February 2003; revised manuscript received 20 October 2003; published 20 February 2004)

Under heating, α-AlF_3 undergoes a structural phase transition from rhombohedral to cubic at temperature T around 730 K. The density-functional method is used to examine the $T=0$ energy surface in the structural parameter space, and finds the minimum in good agreement with the observed rhombohedral structure. The energy surface and electronic wave functions at the minimum are then used to calculate properties including density of states, Γ-point phonon modes, and the dielectric function. The dipole formed at each fluorine ion in the low-temperature phase is also calculated, and is used in a classical electrostatic picture to examine possible antiferroelectric aspects of this phase transition.

DOI: 10.1103/PhysRevB.69.054109 PACS number(s): 64.70.Kb, 71.20.−b, 77.80.Bh

I. INTRODUCTION

The ionic insulator AlF_3 has a number of known polymorphs,[1,2] which all convert irreversibly to the stable α-AlF_3 within the temperature range approximately 730 to 920 K. Recent interest in this material arises due to its catalytic activity for dismutation and halogen-exchange reactions.[3]

Above its transition temperature (about 730 K),[4] α-AlF_3 has the cubic perovskite structure AMX_3, with the A cations absent (or the ReO_3 structure). Aluminum plays the role of the M cation, and is surrounded by an octahedron of corner-shared fluorine atoms. At low temperature, the structure becomes rhombohedral, and this symmetry lowering can be characterized as a rotation of the fluorine octahedron about one of the threefold axis of the perovskite cubic cell (or the $a^-a^-a^-$ system in Glazer's tilt system[5]). As every adjacent octahedron rotates in the opposite sense, the wave vector of this distortion is (π,π,π), and the unit cell becomes double the size of that in the cubic phase.

We study the α-AlF_3 structure by using pseudopotentials, a plane-wave basis, and the local-density approximation (LDA) method. After being tested, the pseudopotentials are applied in bulk α-AlF_3. The total energy surface is examined in the structural parameter space where the cubic phase is compared with the rhombohedral phase found at the deepest nearby minimum of the energy surface.

II. TESTING DIFFERENT PSEUDOPOTENTIALS

The Troullier and Martins method[6] is used to generate the pseudopotentials. Since there are different possibilities of choosing cutoff radii r_{cl}, as well as how many valence orbitals to include in the pseudopotentials, we test the pseudopotentials by doing LDA self-consistent iterations for a crystal or molecule prototype and compare the results with FP-LAPW (Ref. 7) all-electron calculations (full potential linearized augmented plane wave[8]). This provides guidance on the choice of energy cutoff of the plane-wave basis, and also the choice of local potential, in the α-AlF_3 calculation that follows. The results of these tests are shown in Table I and Table II, for aluminum and fluorine separately. For the Ceperley-Alder exchange-correlation energy,[9] the Vosko-Wilk-Nusair[10] parametrization is used.

The test of the aluminum pseudopotential is performed in bulk Al metal, not only the observed fcc structure, but also the simple cubic (sc) and bcc structures, where comparison can still be made between the all-electron method and LDA. The results show that the pseudopotential for the Al^{3+} ion should be capable of describing the unoccupied $3d$ orbital. Otherwise, even the large r_{cl} ($l=0,1$ for s and p orbitals) needed to fix the lattice constant in the fcc aluminum are insufficient to remove the r_{cl} dependence of the lattice constant and bulk modulus. Due to the more attractive nature of the d pseudopotential, including the $3d$ orbital reduces the dependence of these two quantities on r_{cl} and the choice of local potential, and improves the agreement with the all-electron results. Better agreement is also seen in comparisons for sc and bcc structures of Al metal.

The fluorine pseudopotential is tested for the F_2 molecule. Unlike the low plane-wave cutoff needed for aluminum (less than 40 Ry), more than 90 Ry is needed in the F_2 molecule. For bulk Al metal we use a k-point mesh of $12\times12\times12$ that contains 56 special k points, while for F_2 we do a one k-point calculation.

Results in the following sections are calculated using pseudopotentials ($Al^{\dagger}$, $F^{\dagger}$) as shown in the captions of the tables. This set of pseudopotentials gives the lattice constant ($a=5.02$ Å), and bulk modulus ($B=146.6$ GPa) of cubic α-AlF_3 in good agreement with all-electron results ($a=5.043$ Å, $B=150$ GPa).

III. RESULTS FROM LDA

A. k-point test and density of states

A k-point mesh of $3\times3\times3$ is used for the Brillouin-zone summation for α-AlF_3. This is tested for cubic α-AlF_3, where a finer mesh of $4\times4\times4$ gives a barely different energy vs plane-wave cutoff curve, with energy uncertainty less

TABLE I. Aluminum pseudopotential tests on bulk Al. The first column shows the cutoff radii in units of Bohr radius (a_0) for the valence orbitals ($l=0,1,2$). Tests with r_{c2} omitted do not include the d orbital. The following columns show the use of core correction, the choice of local potential, lattice constant, bulk modulus, and the total energy per atom with respect to the fcc structure. Values are shown in atomic units (e denotes electron charge and a_0 denotes Bohr radius). ΔE is defined to be zero for the fcc structure, while the total energy differences between fcc and other structures can be compared with all-electron results. The pseudopotential with a † is chosen for the calculations of α-AlF_3.

$r_{c0}/r_{c1}/r_{c2}$ (a_0)	Core corr.	Local	Lattice const. (a_0)	B ($\times 10^{-3} e^2/a_0^4$)	ΔE (e^2/a_0)
fcc structure					
2.2/2.5	Yes	s	7.738	2.487	0
2.4/2.5	Yes	s	7.712	2.524	0
2.6/2.6	Yes	s	7.672	2.607	0
1.9/2.4/2.7	Yes	d	7.507	2.873	0
1.8/2.2/2.7	Yes	s	7.500	2.850	0
1.8/2.2/2.7	Yes	p	7.516	2.896	0
1.8/2.2/2.7	Yes	d	7.507	2.873	0
1.8/2.2/2.6	Yes	d	7.505	2.934	0
2.6/2.6/2.6†	No	d	7.481	2.865	0
All electron			7.536	2.905	0
Experiment			7.650	2.579	
sc structure					
1.9/2.4/2.7	Yes	d	5.063	2.176	0.01431
1.8/2.2/2.7	Yes	s	5.061	2.170	0.01451
1.8/2.2/2.7	Yes	p	5.069	2.195	0.01425
1.8/2.2/2.7	Yes	d	5.063	2.177	0.01431
1.8/2.2/2.6	Yes	d	5.062	2.175	0.01436
2.6/2.6/2.6†	No	d	5.050	2.072	0.01462
All electron			5.065	2.096	0.01449
bcc structure					
1.9/2.4/2.7	Yes	d	6.015	2.546	0.00368
1.8/2.2/2.7	Yes	s	6.009	2.534	0.00374
1.8/2.2/2.7	Yes	p	6.023	2.581	0.00368
1.8/2.2/2.7	Yes	d	6.015	2.542	0.00368
1.8/2.2/2.6	Yes	d	6.014	2.538	0.00370
2.6/2.6/2.6†	No	d	5.992	2.472	0.00380
All electron			6.027	2.525	0.00414

than 1 meV. This mesh gives six special k points after symmetrization (according to the point group D_{3d} of the crystal), over which we include at least 36 states in the truncated Hamiltonian diagonalization processes. Since in the rhombohedral unit cell of α-AlF_3 we consider the 48 valence electrons from aluminum $3s^2 3p^1$ and fluorine $2s^2 2p^5$, these electrons will occupy the 24 lowest lying bands. A test including more states, 48 states for example, shows that in the process of iterative diagonalization, using 36 states gives convergent answers for the eigenvalues of the lowest 24 bands. Thus we include 36 states in the calculation of the minimum on the energy surface. To make the density-of-states plot, we include 50 states to better describe the empty

TABLE II. Fluorine pseudopotential tests on F_2 molecule. The last column indicates the plane-wave cutoff needed to obtain the convergent result. The pseudopotential with a † is chosen for the calculations of α-AlF_3.

r_{c0}/r_{c1} (a_0)	Core corr.	Local	Bond (a_0)	Force const. (e^2/a_0^3)	Cutoff (Ry)
1.4/1.6	No	p	2.780	0.370	90
1.4/1.45	Yes	p	2.710	0.408	90
1.3/1.3	Yes	s	2.599	0.384	Over 100
1.3/1.3†	No	s	2.603	0.376	90
1.2/1.2	Yes	s	2.617	0.387	Over 100
All electron			2.632	0.376	
Experiment			2.669	0.302	

states from aluminum orbitals. As shown in Fig. 1, LDA gives an insulator band gap of 8 eV. We choose 90 Ry to be the energy cutoff for the plane-wave basis. This choice gives the same energy difference between the two structures as that from the choice of 140 Ry (with error within 1–2 meV. The two structures are the cubic and the rhombohedral structures at the minimum.)

B. Crystal structure

We use LDA to search for the ground state in the rhombohedral symmetry class $R\bar{3}C$ seen experimentally in α-AlF_3.[4] There are three free parameters: (1) the lattice constant a, (2) the angle θ between any two of the rhombohedral lattice vectors, and (3) the inner parameter δ, which describes the bending of the Al-F-Al bond. To describe these three parameters, we first start from the cubic structure with lattice vectors $(2b,0,0)$, $(0,2b,0)$, and $(0,0,2b)$, where b is the Al-F bond length. A rhombohedral unit cell is formed by picking new lattice vectors $\vec{a}_1=(0,2b,2b)$, $\vec{a}_2=(2b,0,2b)$, and $\vec{a}_3=(2b,2b,0)$. The angle θ defined as $\theta=\cos^{-1}(\vec{a}_1\cdot\vec{a}_2/|\vec{a}_1||\vec{a}_2|)$ is 60° in this case. This new cell is then elongated along the [111] direction. Consequently, the strains $\epsilon_{23}=\epsilon_{31}=\epsilon_{12}$ become nonzero, and $\theta\neq 60°$. Viewed from

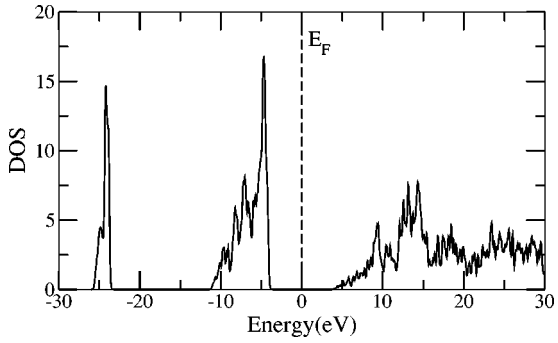

FIG. 1. Density-of-states plot of α-AlF_3 in the rhombohedral ground state, using pseudopotential ($Al^\dagger$, $F^\dagger$). The rhombohedral ground state has unit cell edge 4.76 Å, $\theta=57.5°$, and $\delta=0.098$. This calculation includes 50 states and uses a k-point mesh $6\times6\times6$. The temperature broadening is 54 meV.

the [111] direction, in the aluminum plane the ions form a hexagonal pattern, and the nearest Al-Al distance on this (111) plane is the lattice constant a. This rhombohedral structure can also be described in a hexagonal setting, with the following c/a ratio

$$\frac{c}{a}=\sqrt{\left(\frac{3}{2}\right)\left(\frac{1+2\cos\theta}{1-\cos\theta}\right)}. \tag{1}$$

The cell shape and cell volume V are determined by a and c/a:

$$V=\frac{a^3}{2\sqrt{2}}\sqrt{\frac{1+2\cos\theta}{1-\cos\theta}}=\frac{a^2c}{2\sqrt{3}}, \tag{2}$$

while the relation between the lattice constant a and the length of the rhombohedral lattice vectors is

$$a/|\vec{a}_1|=\sqrt{2(1-\cos\theta)}. \tag{3}$$

There are two aluminum ions and six fluorine ions in each rhombohedral unit cell. The fluorine ions sit at the $6e$ sites $[(x,\overline{x}+\frac{1}{2},\frac{1}{4})$, $(x,x+\frac{1}{2},\frac{3}{4})$, etc.], and $\delta=x-0.75$ is the deviation from $x=0.75$ where the Al-F-Al bond angle is strictly 180°. The distortion caused by δ alone defines the octahedron rotation angle ω about the [111] axis,

$$\tan\omega=2\sqrt{3}\delta. \tag{4}$$

On the other hand, the c/a ratio and the ω have the following relation:

$$\frac{c}{\sqrt{6}a}=\frac{1+\zeta}{\cos\omega}, \tag{5}$$

where ζ describes the flattening ($\zeta<0$) and elongation ($\zeta>0$) of the octahedron along [111].

We first assume cubic symmetry by fixing $\theta=60°$ and $\delta=0$. LDA gives the lattice constant $a=a^*=5.02$ Å for the cubic phase. With the lattice constant kept fixed at the value $a=a^*$, δ is then relaxed to give minimum energy at $(a,\theta,\delta)=(a^*,60°,\pm0.04)$. As shown in Fig. 2, the relaxation of δ finds minima at $\delta=\pm0.04$ and a maximum at $\delta=0$, with an energy difference of 14.4 meV, showing that in our $T=0$ energy surface study, the unbent Al-F-Al bond, and therefore the strictly cubic structure, is not a metastable solution.

The three parameters are then relaxed in turn to approach the deepest nearby minimum. In fact, in the parameter space, there is a path that keeps the fluorine octahedra rigid and leads to the region near the overall minimum. A rigid octahedron means that the Al-F bonds are fixed at the bond length found by LDA in the cubic phase

$$b=\frac{a^*}{2\sqrt{2}}=\frac{a}{2\sqrt{2}\cos\omega} \tag{6}$$

and that the angles between neighboring Al-F bonds are always 90° ($\zeta=0$). With these two restrictions, only one parameter δ remains and defines the rigid octahedron path. The energy along this path is also shown in Fig. 2. The overall minimum locates not far from the minimum on this path. It has an Al-F bond length only 0.3% longer, a pretty small octahedron elongation factor $\zeta=0.25\%$, and the total energy 93 meV lower than the cubic phase. Table III shows the comparisons between LDA and experimental data.[4] While no $T=0$ experimental numbers are available, one can only make reasonable comparisons for the deviation of bond length and ζ. The rhombohdral phase observed in the experiment has an Al-F bond length 0.43% longer than the value observed in the cubic phase, and $\zeta=-0.102\%$ (meaning the octahedron is slightly flattened). This indicates that both the LDA and the experimentally found rhombohedral phases are close to the rigid octahedron path.

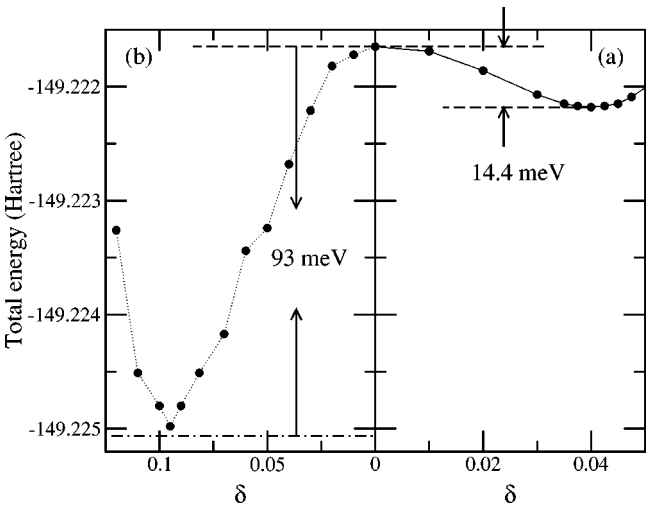

FIG. 2. The relaxation of δ from the cubic structure is shown in plot (a). The curve of total energy (per two formulas of AlF_3) vs δ at $\theta=60.0°$ and $a=5.02$ Å shows that the cubic phase is sitting at an energy maximum. In (b), the curve follows the rigid-octahedron path, and leads to the region near the overall minimum in the parameter space. The dotted-dashed line shows the energy of the overall minimum.

C. Phonon modes

Previous workers[11] investigated the phonon spectrum of the cubic phase using the generalized Gordon-Kim method.[12]

TABLE III. The structure parameters found by LDA are compared with experimental values (Ref. 4) here for different phases. The total energy (per two formulas of AlF_3) difference between the two phases is also shown here, where the total energy of the cubic phase is set to zero. The values for the rhombohedral phase are calculated at the minimum of the energy surface.

	Lattice const. (Å)	$\theta(°)$	δ	ΔE (meV)
psp (Al^+,F^+) rhom	4.76	57.5	0.098	−93
Experiment (LT)	4.9382	58.82	0.0691	
psp (Al^+,F^+) cubic	5.02	60.0	0.0	
Experiment (HT)	5.0549	59.94	0.0129	

TABLE IV. Some of the Γ point phonon mode frequencies calculated by LDA. Direct comparison with experiments is not available since previous observations are done at RT and above. However, in the experiment it is found that the two high-energy E_g modes only weakly depend on temperature. A crude extrapolation using $\omega^2 = A(T - T_c)$ (from Curie-Weiss law and Lyddane-Sachs-Teller relation) and the RT experimental data (Ref. 13) gives the frequency values at $T = 0$.

	A_{1g}	E_g	E_g	E_g
LDA	205	182	350	487
Experiment (RT)	158	98	383	481
Extrapolation	190	118	388	481
	A_{2g}	A_{2g}		
LDA	361	691		

Density-functional theory was applied to construct the charge distribution and polarizability of the ion. An approximate crystal energy is then calculated from the ion results, and is used to examine the crystal-lattice dynamics. However, they did not find an instability of the cubic phase, which is contradictory to the experiment. Here we use full LDA to examine the energy surface around the rhombohedral minimum, and extract the soft phonon modes directly. The rhombohedral minimum described in the preceding section, and the dipole aspect discussed in Sec. IV, both show the instability of the cubic phase.

At the Γ point of the rhombohedral phase, the irreducible representations are those of the point group D_{3d} (note that the space group of the rhombohedral phase is $R\bar{3}C$, which is nonsymmorphic). Among the 12Γ point modes provided by the fluorines, namely, $A_{1g} \oplus 2A_{2g} \oplus 3E_g \oplus A_{1u} \oplus 2A_u \oplus 3E_u$, the four modes $A_{1g} \oplus 3E_g$ are Raman active. Viewed from the cubic phase, the octahedron rotation that governs the structural transition is the R_5 mode (in Kovalev labeling) at the zone boundary (π, π, π).[13] After distortion, the R_5 mode gives rise to the zone center A_{1g} mode and one of the three E_g modes. Raman experiments[13,14] showed that the A_{1g} and one E_g are the soft phonon modes below transition. The A_{1g} is the Al-F-Al bond angle bending mode. Using the fluorine atomic mass, and the energy vs δ curve, the A_{1g} frequency is calculated to be 205 cm^{-1}. We also calculate the other restoring coefficients of the three E_g modes, and the two Raman-inactive A_{2g} modes. Their frequencies are listed in Table IV.

D. Dielectric function

The electronic part of the dielectric tensor $\epsilon(\boldsymbol{q}=0,\omega)$ is also calculated. $\epsilon_{xx} = \epsilon_{yy} \neq \epsilon_{zz}$ is expected since we have chosen lattice vectors such that $\hat{x}$ and $\hat{y}$ are perpendicular to the threefold axis. The imaginary part of the dielectric function can be directly obtained by calculating all direct interband transitions:[15]

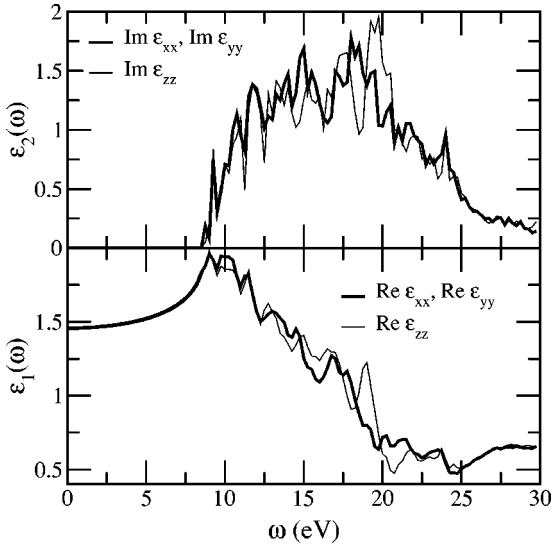

FIG. 3. Plots of dielectric functions. This calculation includes 50 states and uses a *k*-point mesh $6 \times 6 \times 6$.

$$\epsilon_2(\omega) = \left(\frac{2\pi e}{m\omega}\right)^2 \sum_k \sum_{m,n} |\langle \psi_{n,k} | \vec{p} | \psi_{m,k} \rangle|^2 f_n (1 - f_m) \times \delta(E_m - E_n - \hbar\omega), \quad (7)$$

where $\vec{p}$ is the momentum operator, and k runs through all k points in the Brillouin zone allowed in a unit volume. The band indices are m and n, $f_{n,k}$ and $f_{m,k}$ are the occupation numbers of the nth and mth states at the kth k point. The real part of dielectric function is obtained using the Kramers-Kronig relation. The result at $T = 0$ is given in Fig. 3, but we do not know of any experiment to compare with. However, this calculation does neglect the nonlocal potential effect[16] and the local field effect,[17] and follows the pseudo-wavefunctions that are smoothened in the ion core regions.

IV. INNER PARAMETER δ AND DIPOLE FORMATION

The formation of a dipole plays an important role in the energy difference between the two α-AlF_3 structures. When the inner parameter δ is nonzero, each fluorine atom develops a dipole (aluminum atoms sit on inversion centers and therefore cannot have dipoles). Starting from the cubic structure, the distortion from δ alone defines the octahedron rotation angle ω about the [111] axis [see Eq. (4)] and already lowers the symmetry to $R\bar{3}C$. The parameter δ is irrelevant to the c/a ratio, but it does flatten the octahedron [see Eq. (5)]. It also elongates the Al-F bond length, and introduces a polarization to each fluorine. The energy gain from the fluorine dipole-dipole interaction drives the structure off-cubic. This is shown in Fig. 2, where the cubic structure is found to be not a metastable solution.

A naive picture of ionic solids has spherical electron charge clouds of total charge Q_i around the ith ion. In reality, charge clouds are distorted. For example, in high-T cubic α-AlF_3, the F ions are noticeably prolate when examined in a (100)-plane charge-contour calculation.[18] This distortion is

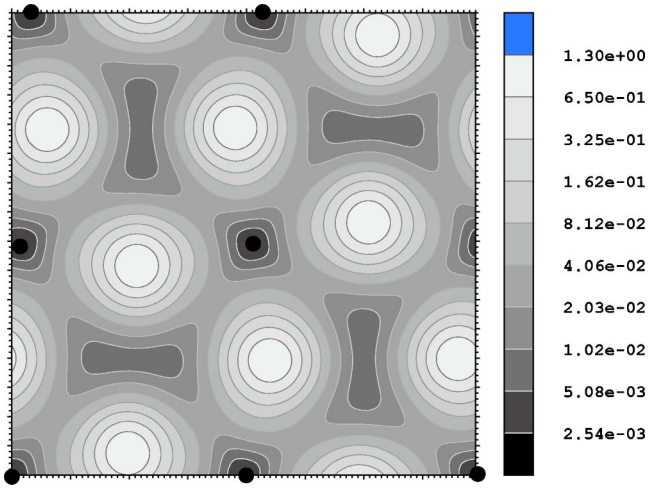

FIG. 4. Charge-density plot of the rhombohedral phase on a (100) plane. The [100] direction is ill-defined since it is inherited from the cubic phase, but the plane shown here does contain the aluminum ions (labeled in solid dots) that form the (100) plane in the cubic phase. The fluorine ions are slightly off the plane shown here, and display clearly a prolate charge distribution.

still evident in the low-T rhombohedral phase, as shown in Fig. 4. The value of the charge Q_i, on the other hand, is not uniquely definable. By creating a sphere centered at each fluorine atom, with a radius that only allows neighboring spheres in the rhombohedral phase to touch each other at one point, we define a volume to examine the charge and the dipole moment of the fluorine. In the cubic phase, such a sphere contains charge $-0.675|e|$, while it contains $-0.68|e|$ in the rhombohedral phase (with a slightly different radius). Using the same sphere, we compute the local induced dipole moment $\mathbf{p}_{\mathrm{ind}}$ of the fluorine ion (which also has no unique definition).[19] As expected from symmetry, $p_{\mathrm{ind}}=0$ in the cubic phase, whereas $p_{\mathrm{ind}}=0.103|e|$Å in the rhombohedral phase, pointing from the fluorine position of the unbent Al-F-Al bond towards the actual distorted fluorine position. Note that the displacive dipole is $p_{\mathrm{dis}}=0.315|e|$Å, defined by the fluorine charge $-0.675|e|$ and the displacement 0.467 Å of the fluorine ion when the Al-F-Al bonds bend. By symmetry, the other fluorine sitting at the opposite side of the octahedron has its dipole pointing exactly in the opposite direction. Therefore the material could be called antiferroelectric.[20]

The dipoles and charges can as well be determined by doing integration in one of the equivalent polyhedra that surround the F^- ions and partition the whole space (the Al^{3+}'s sit on shared vertices of the F^- polyhedra). In this way, the ions are charged as Al^{3+} and F^-, while $p_{\mathrm{ind}}=0.0963|e|$Å and $p_{\mathrm{dis}}=0.467|e|$Å.

It is worthwhile to see if a simplified picture with these numbers helps to understand the energy. In LDA, the energy includes the exact electrostatic or Hartree energy from the electron charge clouds, as well as other quantum effects (energy of delocalization, exchange, and correlation). Purely classical electrostatic models (plus hard-core repulsion), on the other hand, provide a simple but useful view. We shall see how much classical electrostatic energy comes from the charge and if this helps to explain the stability of the structural deformation.

In a simplified picture where only electrostatic energy and dipole formation energy [E_1 in Eq. (8), where $\alpha=0.858$ Å^3 (Ref. 21)] are considered, the total energy is

$$\begin{aligned} E &= E_1+E_2+E_3+E_4 \\ &= \sum_i \frac{\boldsymbol{p}_i^2}{2\alpha} + \sum_i \sum_{j<i} \frac{Z_i Z_j}{r_{ij}} + \sum_i \sum_{j<i} \frac{Z_i(\boldsymbol{p}_j\cdot\boldsymbol{r}_{ij})}{r_{ij}^3} \\ &\quad + \sum_i \sum_{j<i} \frac{\boldsymbol{p}_i\cdot\boldsymbol{p}_j - 3(\hat{\boldsymbol{r}}_{ij}\cdot\boldsymbol{p}_i)(\hat{\boldsymbol{r}}_{ij}\cdot\boldsymbol{p}_j)}{r_{ij}^3}. \end{aligned} \tag{8}$$

This form leaves out the quantum effects and the effect from covalent bond angle. We find that E_2, which is purely ionic electrostatic (including displacive dipoles), is less negative in the rhombohedral structure than in the cubic structure (i.e., if the same ion charge assignment is considered in both cases). However, when the induced-dipole-related terms ($E_1+E_3+E_4$) are also considered, the energy is lowered. By assuming point charges and point dipoles, we use the results from the polyhedron method to illustrate this picture: E_2 per two AlF_3 formulas in the rhombohedral phase is 1 eV higher than that in the cubic phase; but E_3 and E_4 bring the energy E down, with the cost of E_1, to 0.97 eV lower than the cubic phase (which has only E_2.) This suggests that the effect of induced dipoles is more than enough to compensate the energy loss from the structural distortion.

V. CONCLUSION

We report a LDA study of bulk α-AlF_3. By examining the $T=0$ energy surface for structures of the phases on both sides of the transition, we find the structural parameters to agree with previous experiments, and the cubic phase not to be a metastable solution. Using the result of LDA, the density of states plot and the dielectric function are provided. At the Γ point, the predicted A_{1g} soft phonon mode and E_g modes are compared with previous Raman experiment, while two other A_{2g} modes are predicted. We look at the charge and dipole moment at each fluorine ion, and use these quantities to calculate the classical electrostatic energy. In the antiferroelectric distortion which accompanies the structural transition, a classical calculation shows that the electrostatic energy gain from dipoles is more than enough to compensate the energy loss from the ion-array deformation.

ACKNOWLEDGMENTS

We thank C. Gray and S. Chaudhuri for suggesting the project and for helpful discussions. The LDA code (BEST) and the FT-LAPW code are provided by Brookhaven National Laboratory. Work at Stony Brook was supported in part by NSF Grant No. DMR-0089492. Work at Columbia was supported in part by the MRSEC Program of the National Science Foundation under Grant No. DMR 0213574.

*Current address: IBM Research Division, T. J. Watson Research Center, Yorktown Heights, New York, 10598.

[1] N. Herron, D.L. Thorn, R.L. Harlow, G.A. Jones, J.B. Parise, J.A. Fernandez-Baca, and T. Vogt, Chem. Mater. **7**, 75 (1995).
[2] C. Alonso, A. Morato, F. Medina, F. Guirado, Y. Cesteros, P. Salagre, and J.E. Sueiras, Chem. Mater. **12**, 1148 (2000).
[3] E. Kemnitz and L.E. Manzer, Prog. Solid State Chem. **26**, 97 (1998).
[4] P.J. Chupas, M.F. Ciraolo, J.C. Hanson, and C.P. Grey, J. Am. Chem. Soc. **123**, 1694 (2001).
[5] P.M. Woodward, Acta Crystallogr., Sect. B: Struct. Sci. **B53**, 32 (1997).
[6] N. Troullier and J.L. Martins, Phys. Rev. B **43**, 1993 (1991).
[7] P. Blaha, K. Schwarz, G.K.H. Madsen, D. Kvasnicka, and J. Luitz, *WIEN2K, An augmented plane wave plus local orbitals program for caluclating crystal properties* (Vienna University of Technology, Austria, 2001).
[8] D.J. Singh, *Planewaves, Pseudopotentials and the LAPW Method* (Kluwer Academic, Boston, 1994).
[9] D.M. Ceperley and B.J. Alder, Phys. Rev. Lett. **45**, 566 (1980).
[10] S.H. Vosko, L. Wilk, and M. Nusair, Can. J. Phys. **58**, 1200 (1980); L. Wilk and S.H. Vosko, J. Phys. C **15**, 2139 (1982).
[11] V.I. Zinenko and M.G. Zamkova, Phys. Solid State **42**, 1348 (2000).
[12] O.V. Ivanov and E.G. Maksimov, Zh. Eksp. Teor. Fiz. **108**, 1841 (1995) [JETP **81**, 1008 (1995)].
[13] P. Danial, A. Bulou, M. Rousseau, J. Nouet, J.L. Fourquet, M. Leblanc, and R. Burriel, J. Phys.: Condens. Matter **2**, 5663 (1990).
[14] P. Danial, A. Bulou, M. Rousseau, and J. Nouet, Phys. Rev. B **42**, 10 545 (1990).
[15] P. Yu and M. Cardona, *Fundamentals of Semiconductors*, 2nd ed. (Springer, New York, 1999), p. 251.
[16] B. Adolph, V.I. Gavrilenko, K. Tenelson, F. Bechstedt, and R. Del Sole, Phys. Rev. B **53**, 9797 (1996).
[17] M.S. Hybertsen and S.G. Louie, Phys. Rev. B **35**, 5585 (1987).
[18] This was pointed out to us by P. Madden (private communication), and later also appeared in our charge contour plot.
[19] L. Bernasconi, P.A. Madden, and M. Wilson, PhysChemComm **5**, 1 (2002).
[20] R. Blinc and B. Žekš, in *Soft Modes in Ferroelectrics and Antiferroelectrics*, edited by E.P. Wohifarth (North-Holland, Amsterdam, 1974).
[21] C. Kittel, *Introduction to Solid State Physics*, 7th ed. (Wiley, New York, 1996), p. 391, and references therein.